materials

MDPI

Article

Incommensurately Modulated Crystal Structure and Photoluminescence Properties of Eu_2O_3- and P_2O_5-Doped Ca_2SiO_4 Phosphor

Hiromi Nakano [1,2,*], Shota Ando [2], Konatsu Kamimoto [2], Yuya Hiramatsu [3], Yuichi Michiue [4], Naoto Hirosaki [4] and Koichiro Fukuda [3]

1 Cooperative Research Facility Center, Toyohashi University of Technology, Toyohashi 441-8580, Japan
2 Department of Applied Chemistry and Life Science, Toyohashi University of Technology, Toyohashi 441-8580, Japan; s183404@edu.tut.ac.jp (S.A.); k163413@edu.tut.ac.jp (K.K.)
3 Department of Life Science and Applied Chemistry, Nagoya Institute of Technology, Nagoya 466-8555, Japan; 30411131@stn.nitech.ac.jp (Y.H.); fukuda.koichiro@nitech.ac.jp (K.F.)
4 National Institute for Materials Science, Tsukuba 305-0044, Japan; michiue.yuichi@nims.go.jp (Y.M.); hirosaki.naoto@nims.go.jp (N.H.)
* Correspondence: hiromi@crfc.tut.ac.jp; Tel.: +81-532-44-6606

Received: 14 November 2019; Accepted: 18 December 2019; Published: 20 December 2019



Abstract: We prepared four types of Eu_2O_3- and P_2O_5-doped Ca_2SiO_4 phosphors with different phase compositions but identical chemical composition, the chemical formula of which was $(Ca_{1.950}Eu^{3+}_{0.013}\square_{0.037})(Si_{0.940}P_{0.060})O_4$ (□ denotes vacancies in Ca sites). One of the phosphors was composed exclusively of the incommensurate (IC) phase with superspace group $Pnma(0\beta0)00s$ and basic unit-cell dimensions of a = 0.68004(2) nm, b = 0.54481(2) nm, and c = 0.93956(3) nm (Z = 4). The crystal structure was made up of four types of β-Ca_2SiO_4-related layers with an interlayer. The incommensurate modulation with wavelength of $4.110 \times b$ was induced by the long-range stacking order of these layers. When increasing the relative amount of the IC-phase with respect to the coexisting β-phase, the red light emission intensity, under excitation at 394 nm, steadily decreased to reach the minimum, at which the specimen was composed exclusively of the IC-phase. The coordination environments of Eu^{3+} ion in the crystal structures of β- and IC-phases might be closely related to the photoluminescence intensities of the phosphors.

Keywords: optical materials; phase transitions; dicalcium silicate; phase compositions; incommensurate structures

1. Introduction

Rare-earth doped dicalcium silicate (Ca_2SiO_4, C_2S) polymorphs have been the subject of extensive study because of the promising applicability of stabilized high-temperature modifications to the phosphor materials of white light-emitting LEDs [1–8]. The red light emission is characteristic of the Eu^{3+}-activated phosphors, due to the transition of the $^5D_0$–$^7F_2$ for Eu^{3+} ion [3,4]. The photoluminescence (PL) originates from the 4f–4f dipole transitions and, hence, the emission wavelengths are nearly the same among the various types of phosphors with different host materials. However, the PL intensity has been tunable for Eu^{3+}-activated lithium tantalite-based phosphors by controlling the coordination environments of the Eu^{3+} ion [9,10]. Accordingly, we speculated that the PL intensities could be also tunable for the Eu^{3+}-activated C_2S phosphors, depending on the polymorphs stabilized at ambient temperature.

The C_2S polymorphs established so far are, in order of increasing temperature, γ (orthorhombic), β (monoclinic), α'_L (orthorhombic), α'_H (orthorhombic), and α (trigonal) [11]. The transformation

temperatures during the heating process are 963 K for β-to-α'_L, 1433 K for α'_L-to-α'_H, and 1698 K for α'_H-to-α. The phase change from α'_L to β on cooling has been reported to be thermoelastic martensitic [12]. Thus, the two phases coexisted at temperatures between the transformation starting temperature (=M_s) and finishing temperature (=M_f), both of which steadily decreased, even below ambient temperature (=T_a), with increasing concentration of dopants in C_2S. The stabilized phases at T_a systematically changed from β ($T_a < M_f$), β + α'_L ($M_f < T_a < M_s$) to α'_L ($M_s < T_a$) with increasing concentrations of foreign ions such as Sr^{2+} or P^{5+} [13,14]. In the crystal structure of β-Ca_2SiO_4 there are two types of Ca sites. One (Ca1 site) is surrounded by seven O atoms, and the other (Ca2 site) has an eight-fold coordination [15]. When activated by Eu^{3+} ions, the ions enter both Ca1 and Ca2 sites to generate $^5D_0$–$^7F_0$ emission peaks at 270 nm excitation [16].

In addition to the five types of polymorphs previously mentioned, an incommensurate (IC) phase has been reported to occur for the P_2O_5-doped C_2S [17–20]. The modulation wavevector, $N^{-1} \times \mathbf{b}^*$, has been along the *b*-axis of the underlying orthorhombic basic structure, where *N* is a noninteger. Saalfeld and Klaska prepared the IC-phase with $N = 3.75$, and determined the atom arrangements within the hypothetical supercell of $4 \times b$ based on the space group $Pnm2_1$ [17]. Recently, the incommensurately modulated crystal structure of $(Ca_{1.88}Eu^{2+}_{0.01}\square_{0.11})(Si_{0.78}P_{0.22})O_4$ ($N = 3.649$) [20], where □ denotes a vacancy in Ca site, has been determined, using a (3 + 1)-dimensional description based on the superspace formalism [21,22].

In the present study we have, for the first time, clarified the PL properties of the Eu^{3+}-activated IC-phase phosphor, the chemical formula of which was $(Ca_{1.950}Eu^{3+}_{0.013}\square_{0.037})(Si_{0.940}P_{0.060})O_4$. The incommensurately modulated crystal structure was determined from the X-ray powder diffraction data using a (3 + 1)-dimensional description based on the superspace group $Pnma(0\beta0)00s$. The sintered specimen was subject to different heat treatments in air at 1473–1773 K. We demonstrated a close relationship between the phase composition (consisting of β, α'_L, and IC) and PL intensity.

2. Materials and Methods

The materials were synthesized by solid-state reaction. A powder mixture with atom ratios of [Ca:Eu:Si:P] = [1.950:0.013:0.940:0.060] was prepared from reagent chemicals of $CaCO_3$, SiO_2, $CaHPO_4{\cdot}2H_2O$, and Eu_2O_3 (>99.9% grade). Together with a small amount of acetone, it was thoroughly mixed in a planetary ball mill (Pulverisette P-6, Fritsch, Germany). The ZrO_2 balls, with 2 mm diameter, were used in the mill at a rotation speed of 400 rpm. The mixed specimens were pressed into pellets and heated at 498 K for 6 h, 973 K for 2 h, and then 1273 K for 8 h in air. The disc-shaped sintered specimens, the chemical formula of which corresponds to $(Ca_{1.950}Eu^{3+}_{0.013}\square_{0.037})(Si_{0.940}P_{0.060})O_4$, were subsequently annealed at four different temperatures (1473, 1573, 1673, and 1773 K) for 4 h in air, followed by quenching in water. The stable phases during the annealing processes were α at 1773 K and α'_H at 1473–1673 K. We examined the specimens with a scanning electron microscope equipped with an energy-dispersive spectrometer to measure grain sizes and to confirm homogeneity.

Phase identification was made based on the X-ray diffraction (XRD) data ($CuK\alpha_{1+2}$), which were obtained using an X-ray powder diffractometer (RINT 2500, Rigaku Co., Ltd., Japan) operated at 40 kV and 200 mA. The phase compositions, as well as the crystal structure of the IC-phase, were determined by the Rietveld method [23] from the X-ray profile intensity data ($CuK\alpha_1$) collected at 298 K on another diffractometer (X'Pert PRO Alpha-1, PANalytical B.V., Almelo, the Netherlands), operated at 45 kV and 40 mA. We quantitatively determined the phase compositions of the samples using the phase-analysis method (2θ range of 25.0°–43.0°) based on Brindley's procedure [24], the subroutine of which was implemented in the computer program RIETAN-FP [25] based on the structural parameters reported by Jost et al. [15] for the β-phase, Udagawa et al. [26] for the α'_L-phase, and Saalfeld and Klaska [17] for the IC-phase having a supercell of $4 \times b$. We used the computer programs JANA2006 [27] for the detailed structural analysis of the IC-phase (2θ range of 5.010°–147.981°), and VESTA [28] for the crystal structure drawing. Distortion parameters for the coordination polyhedra of the β-phase were determined using the computer program IVTON [29].

Excitation and emission spectra were obtained using a fluorescence spectrophotometer (F-7000, HITACHI, Japan).

3. Results and Discussion

3.1. Constituent Phases and Crystal Structure of IC-Phase

Figure 1 shows a series of XRD patterns of $(Ca_{1.950}Eu^{3+}_{0.013}\square_{0.037})(Si_{0.940}P_{0.060})O_4$ phosphors annealed at different temperatures. For the specimen annealed at 1473 K, the phase composition was 70.7 mol % β and 29.3 mol % α'_L (Figure 2a). The specimen annealed at 1773 K was composed exclusively of the IC-phase, as evidenced from the satisfactory pattern fitting result (Figure 2b), although the structural model used was of the commensurate structure with the supercell of $4 \times b$. This implies that the modulation wavevector of the IC-phase should be close to 0.25 (=1/4) × **b***. In fact, we found it to be 0.2433(2) × **b*** as discussed later, and hence there were slight positional shifts in Figure 2b from the proper positions for the weak reflections (e.g., 330 and $\overline{3}30$ reflections with $2\theta \approx 31.05°$, and 530 and $\overline{5}30$ reflections with $2\theta \approx 35.23°$) ascribed to the superstructure. Based on the present structural model, the specimens annealed at 1573–1773 K were free from the α'_L-phase. The relative amount of the IC-phase with respect to the β-phase steadily increased when the annealing temperature was increased from 1473 to 1773 K (Table 1).

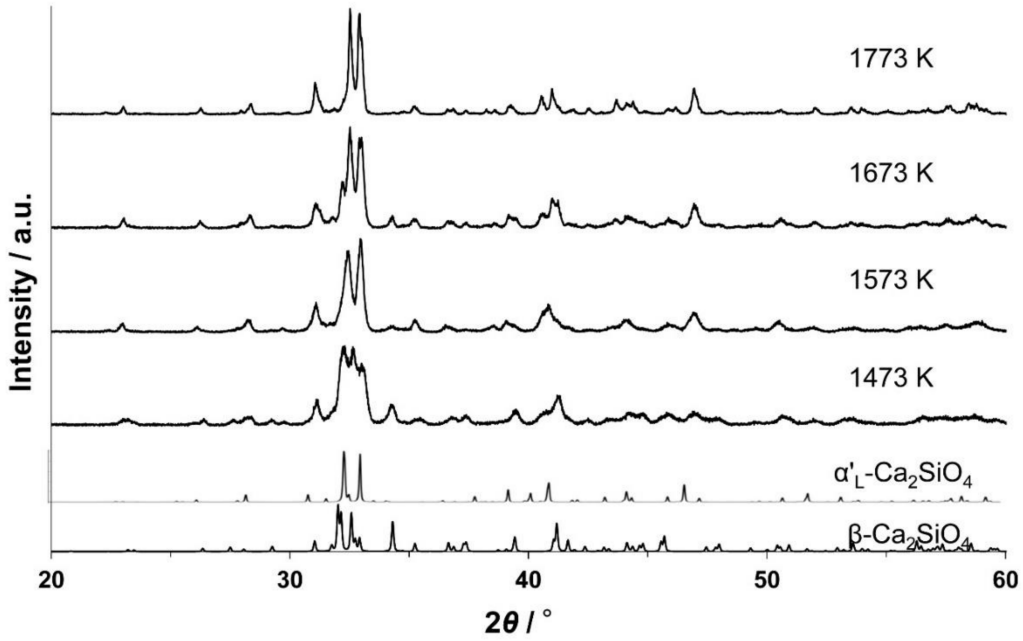


Figure 1. X-ray diffraction (XRD) patterns of samples annealed at 1473–1773 K.

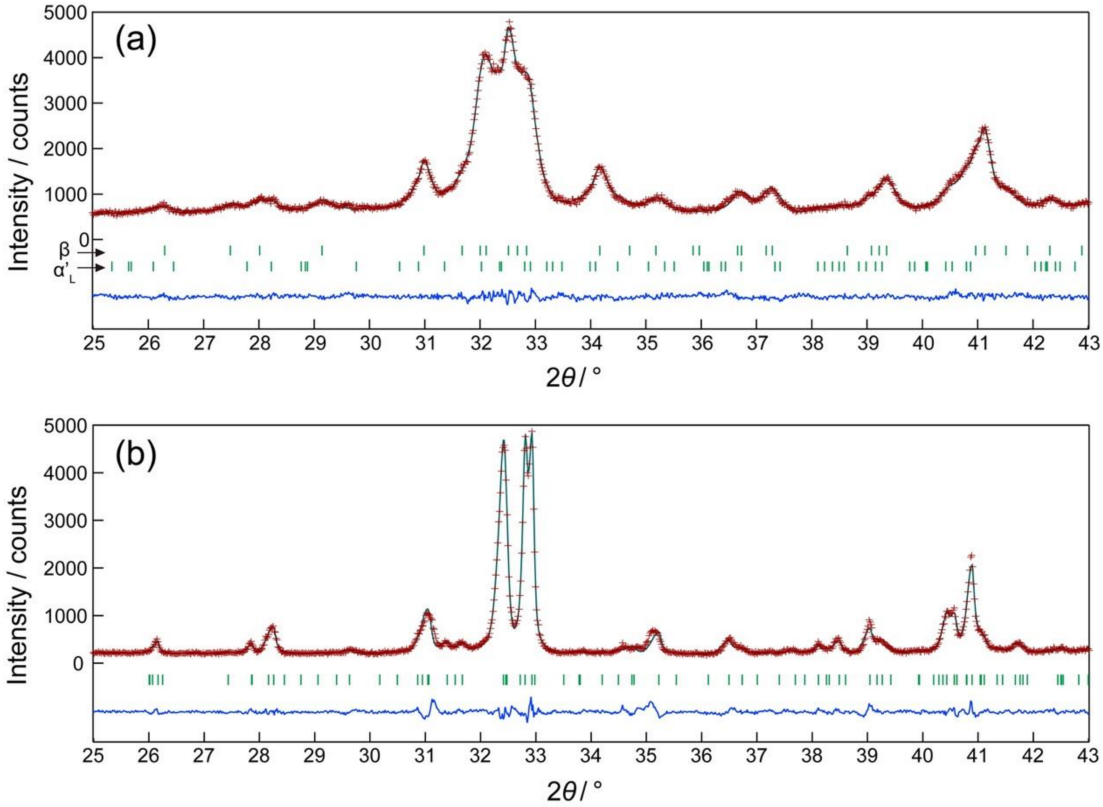


Figure 2. Comparison of the observed diffraction patterns (symbol: +) with the corresponding calculated patterns (upper solid line). The difference curve is shown in the lower part of each diagram. The vertical bars indicate the positions of possible Bragg reflections. The profile intensities were collected for samples annealed at (**a**) 1473 K and (**b**) 1773 K.

Table 1. Changes in phase compositions for the samples annealed at 1473–1773 K. IC: incommensurate.

Phase / K	β	α′L	IC
1473	70.7 mol %	29.3 mol %	-
1573	18.9 mol %	-	81.1 mol %
1673	8.5 mol %	-	91.5 mol %
1773	-	-	100 mol %

We refined the incommensurately modulated structure starting from the initial structural model (superspace group *Pnma*(0β0)00*s*) that was equivalent to the crystal structure of $(Ca_{1.88}Eu^{2+}_{0.01}\square_{0.11})(Si_{0.78}P_{0.22})O_4$ [20]. The refinement resulted in the satisfactory reliability indices of R(all) = 0.0326, Rw(all) = 0.0413, and S(all) = 2.99 (Figure S1). The crystallographic data and the structural parameters are summarized in Tables 2 and 3, respectively. The basic structure contains two nonequivalent Ca sites, Ca1 and Ca2. In the average structure, the site occupation factors of both sites were fixed at 0.9750 for Ca, 0.0065 for Eu, and 0.0185 for vacancy. We tried to demonstrate the occupational modulation in all ranges of t (= $x_4 - \mathbf{q} \times \mathbf{r}$, where x_4 is the fractional coordinate of the 4th direction in superspace description, **q** is the modulation wavevector, and **r** is the positional vector) at these sites to clarify the locations where the Eu^{3+} ions concentrate. However, it remained unclear, because the bond valence sums are nearly the same between Ca^{2+} and Eu^{3+}. Figure 3 shows a partial structure of IC-$(Ca_{1.950}Eu^{3+}_{0.013}\square_{0.037})(Si_{0.940}P_{0.060})O_4$. The *M* site, which is occupied by Si

and P, is coordinated by 4 O ions to form an isolated [MO_4] tetrahedron. The ratio of P/(P + Si) is fixed at 0.06 for the *M* site.

Table 2. Crystallographic data of IC-phase.

Chemical Formula	$\mathbf{(Ca_{1.950}Eu^{3+}{}_{0.013}\square_{0.037})(Si_{0.940}P_{0.060})O_4}$
Crystal system	Orthorhombic
Superspace group	*Pnma*(0β0)00*s*
a/nm	0.68004(2)
b/nm	0.54481(2)
c/nm	0.93956(3)
Modulation wavevector	0.2433(2) × **b***
V/nm^3	0.34810(2)
Z	4
D_x/Mgm^{-3}	3.289

Table 3. Structural parameters of the basic structure for IC-($Ca_{1.950}Eu^{3+}{}_{0.013}\square_{0.037}$)($Si_{0.940}P_{0.060}$)$O_4$.

Site	x	y	z	U_{iso} (×10^{-2} nm^2)	**sof**
Ca1	0.1680(3)	1/4	0.4243(4)	0.0270(10)	Ca/Eu: 0.9750/0.0065
Ca2	0.4935(3)	1/4	0.7106(2)	0.0139(7)	Ca/Eu: 0.9750/0.0065
M	0.2240(4)	1/4	0.0755(6)	0.0134(10)	Si/P: 0.940/0.060
O1	0.3213(12)	1/4	0.9305(9)	0.025(3)	1
O2	0.2994(8)	0.0092(12)	0.1471(7)	0.0181(18)	1
O3	−0.0059(10)	1/4	0.0731(13)	0.038(3)	1

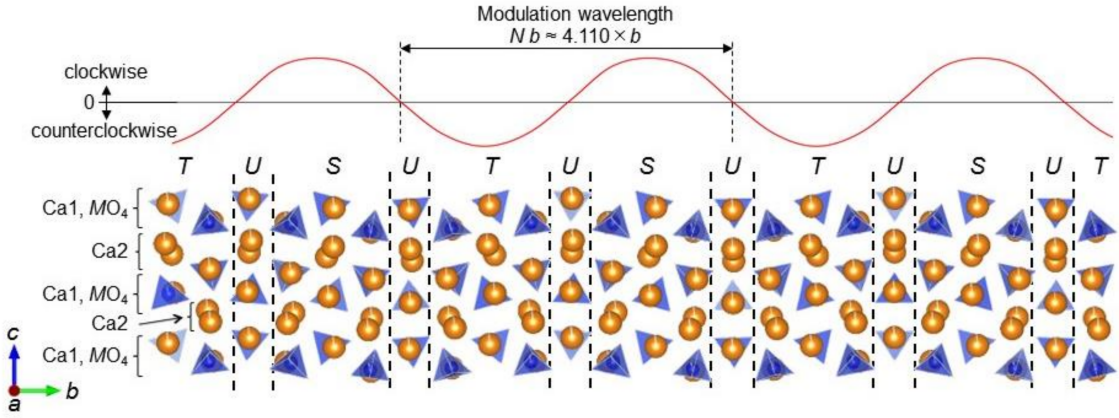


Figure 3. Projection of a partial structure along the *a*-axis.

The present crystal structure is in accord with that of IC-($Ca_{1.88}Eu^{2+}{}_{0.01}\square_{0.11}$)($Si_{0.78}P_{0.22}$)$O_4$, characterized by the tilting of [MO_4] tetrahedra [20], and hence it can be regarded as being made up of five types of layers (denoted by *S*, *S*″, *T*, *T*″, and *U*) that include the [MO_4] tetrahedra with different tilting directions and angles (= Θ) (Figure S2). With layer *S*, the tilting directions of the constituent [MO_4] tetrahedra are, when viewed along [$\bar{1}$00], clockwise with 5° ≤ Θ < 16°. The other type of layer, *T*, contains tetrahedra of counterclockwise tilting and −16° < Θ ≤ −5°. The slightly tilted [MO_4] tetrahedra, with |Θ| < 5°, is characteristic of the interlayer *U*. The atom arrangements of layer *S* and those of *T*, which are similar to the partial crystal structure of β-Ca_2SiO_4 [15], are approximately related by a mirror plane perpendicular to the *b*-axis of *Pnma*(0β0)00*s*. The thicknesses of these layers correspond to one-and-a-half the d_{100}-value of β-Ca_2SiO_4. Although it is very rare, there are *S*″ and *T*″ layers with a thickness almost twice the d_{100}-value. A repetitive sequence of the bundled *SUTU* layer eventually constructs the commensurate structure having the supercell of 4 × *b*. The present incommensurately modulated structure with the wavelength of 4.110 × *b* is formed by the occasional replacements of *S* with *S*″ and/or *T* with *T*″ in the commensurate structure (Figure S3). Since the

modulated structures are definitely ordered ones, the connecting sequence of all these layers is strictly defined by the modulation function. In the crystal structure of IC-$(Ca_{1.88}Eu^{2+}_{0.01}\square_{0.11})(Si_{0.78}P_{0.22})O_4$ with the modulation wavelength of $3.649 \times b$ [20], there are two other layers of *S*′ and *T*′, the thicknesses of which are almost equal to the d_{100}-value of β-Ca_2SiO_4. These layers have never been recognized in the present IC-phase.

In previous studies, a negative linear correlation has been reported between the *N*- and P/(P+Si)-values for the P_2O_5-doped C_2S [14,19]. The larger *N*-value for $(Ca_{1.950}Eu^{3+}_{0.013}\square_{0.037})(Si_{0.940}P_{0.060})O_4$ (N = 4.110) than for $(Ca_{1.88}Eu^{2+}_{0.01}\square_{0.11})(Si_{0.78}P_{0.22})O_4$ (N = 3.649) would be principally induced by the smaller P/(P+Si)-value of the former material as compared with the latter.

3.2. PL Properties Associated with Phase Compositions

Figure 4 shows the emission and excitation spectra of the four types of Eu^{3+}-activated phosphors annealed at 1473–1773 K. Under excitation at 394 nm, the red light was emitted due to the $^7F_0$–$^5L_6$ intraconfigurational transition of Eu^{3+}. The sharp and strong emission peaks appeared at around 594 nm ($^5D_0$–$^7F_1$, magnetic dipole), 625 nm ($^5D_0$–$^7F_2$, electric dipole), and 706 nm ($^5D_0$–$^7F_4$, electric dipole).

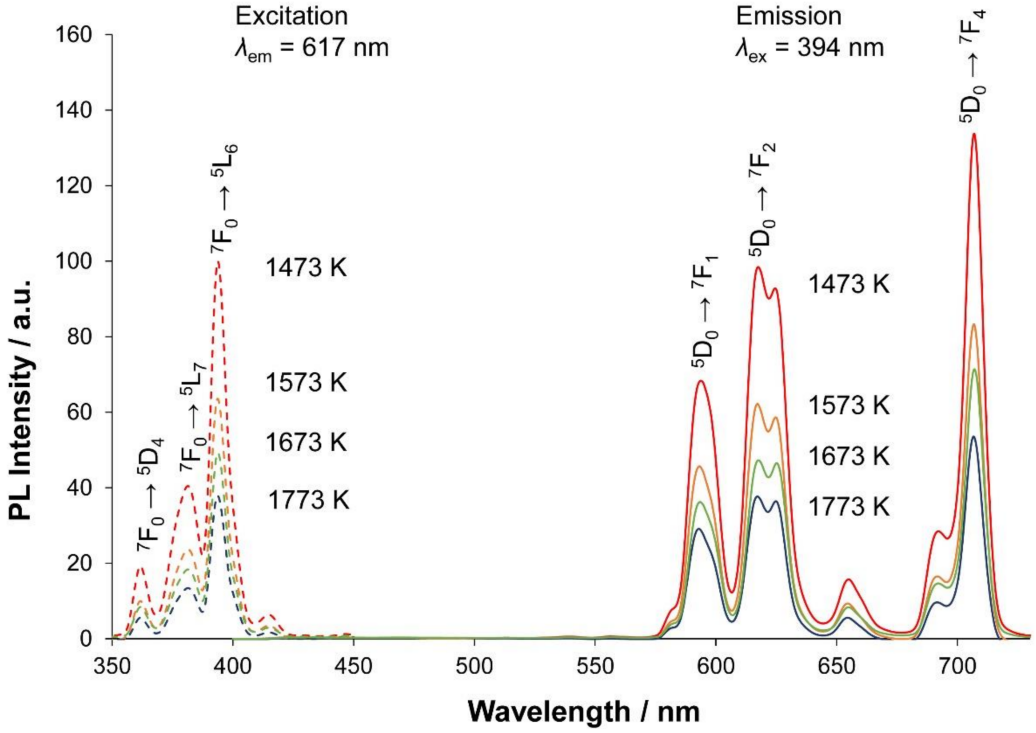


Figure 4. Emission and excitation spectra of the samples annealed at 1473–1773 K.

In this paper, we controlled the phase compositions by annealing at different temperatures in order to investigate the relationship between the crystal structures and PL intensities. The PL intensity steadily decreased with increasing annealing temperature (Figure 4). This implied that the phase compositions of the Eu^{3+}-activated phosphors readily affected the PL intensities. Actually, the intensity was highest for the specimen annealed at 1473 K, the constituent phases of which were β and α'_L, as described previously. With increasing relative amount of the IC-phase with respect to the coexisting β-phase (Table 1), the PL intensity of the phosphor steadily decreased to reach the minimum, at which the specimen was composed exclusively of the IC-phase. As reported previously [8], the PL intensity has also been related to the relative amount of the α'_L phase with respect to the β phase.

In previous studies for the Eu^{3+}-activated lithium tantalite-based phosphors, the centroid-to-cation distance (=eccentricity) of [(Li, Eu)O_{12}] polyhedra was associated with increased efficiency of the red light emission [9,10]. The larger the magnitude of eccentricity became, the stronger the PL intensity of the emission became. In a similar manner, the eccentricity of the Eu^{3+} position in the crystal structure of P_2O_5-doped C_2S phosphors could also be closely related to the PL intensity. We hypothesized that the eccentricity values of [(Ca, Eu)O_n] polyhedra (n is the coordination number) in IC-$(Ca_{1.950}Eu^{3+}{}_{0.013}\square_{0.037})(Si_{0.940}P_{0.060})O_4$ might be smaller compared to those of the Eu^{3+}-activated β-phase, which would eventually cause a much weaker PL intensity for the former than for the latter.

With β-Ca_2SiO_4, the Eu^{3+} ions occupied both Ca1 and Ca2 sites [15]. The eccentricity values were 0.044 and 0.022 nm for the polyhedra [Ca1O_7] and [Ca2O_8], respectively. The maximum bond lengths were 0.280 nm for Ca1–O and 0.279 nm for Ca2–O. With the present IC-phase, the Ca1 and Ca2 sites in the layer *U* were located at t = 0.189 and 0.689. They formed [Ca1O_n] and [Ca2O_n] polyhedra with n = 6, 7, or 8. The Ca sites, situated in the middle parts of the layers *S* (t = 0.439) or *T* (t = 0.939), formed the polyhedra of [Ca1O_n] (n = 7) and [Ca2O_n] (n = 8). The eccentricity values of these polyhedra with different n- and t-values are summarized in Table 4. With Ca1 sites, the eccentricity values were larger for the β-phase (=0.044 nm) than for the IC-phase at t = 0.689 (=0.031 nm). Furthermore, the eccentricity value of the IC-phase at t = 0.189 (=0.009 nm) was much smaller than that of the β-phase (=0.022 nm) for the Ca2 sites. Accordingly, the Eu^{3+} ions that contribute to the relatively weak red light emission intensity of the IC-phase could preferentially occupy those Ca sites.

Table 4. Centroid-to-cation distance (eccentricity) of [CaO_n] polyhedra for IC-$(Ca_{1.950}Eu^{3+}{}_{0.013}\square_{0.037})(Si_{0.940}P_{0.060})O_4$.

Site	t	n	Ca–O Max. (nm)	Eccentricity (nm)	Layer
Ca1	0.189	7	0.280	0.054	*U*
Ca1	0.189	6	0.267	0.105	*U*
Ca1	0.689	8	0.294	0.041	*U*
Ca1	0.689	7	0.273	0.031	*U*
Ca1	0.439	7	0.280	0.041	*S*
Ca1	0.939	7	0.280	0.041	*T*
Ca2	0.189	7	0.259	0.009	*U*
Ca2	0.689	6	0.258	0.040	*U*
Ca2	0.439	8	0.279	0.023	*S*
Ca2	0.939	8	0.279	0.023	*T*

Phase parameter t is defined by $t = x_4 - \mathbf{q} \times \mathbf{r}$, where x_4 is the fractional coordinate of the 4th direction in (3 + 1)-dimensional superspace description, **q** is the modulation wavevector, and **r** is the positional vector.

4. Conclusions

Four types of red-light-emitting phosphors, with different phase compositions but identical chemical composition, were prepared. A close relationship was suggested between the coordination environments of the Eu^{3+} ion in the crystal structures of the β- and IC-phases and their PL properties.

1. The β- and α'_L-phases coexisted for the specimen annealed at 1473 K. With increasing annealing temperature, the relative amount of the IC-phase with respect to the β-phase steadily increased. The specimen annealed at 1773 K was composed exclusively of the IC-phase.
2. The incommensurately modulated crystal structure was determined using a (3 + 1)-dimensional description based on the superspace group *Pnma*(0β0)00*s*. It was composed of β-phase like layers (*S*, *S*″, *T*, and *T*″) and the interlayer (*U*). The *S* and *S*″ layers included the [MO_4] tetrahedra (M = Si or P) tilted clockwise when viewed along [$\bar{1}$00]. Those of *T* and *T*″ contained the tetrahedra tilted counterclockwise. The interlayer *U* was characterized by a slightly tilted tetrahedra. The incommensurate modulation, with modulation wavevector of 0.2433(2) × **b***, was induced by the long-range stacking order of these layers.

3. The PL intensity was the highest for the specimen consisting of both β- and α'_L-phases. As the relative amount of the IC-phase increased with respect to the coexisting β-phase, the PL intensity steadily decreased. The eccentricity of the Eu^{3+} position in the crystal structures of the β- and IC-phases could be closely related to the PL intensities.

Supplementary Materials: The following are available online at http://www.mdpi.com/1996-1944/13/1/58/s1, Figure S1: Comparison of the observed diffraction pattern of $(Ca_{1.950}Eu^{3+}{}_{0.013}\square_{0.037})(Si_{0.940}P_{0.060})O4$ (symbol: +) with the corresponding calculated pattern (upper solid line). The difference curve is shown in the lower part of the diagram. Vertical bars indicate the positions of Bragg reflections. Figure S2: Tilting of the $[MO_4]$ tetrahedron evaluated by the angle Θ. (a) The tilting angles Θ_1 (red line) and Θ_2 (blue line) with t. Because the differences between Θ_1 and Θ_2 in the whole regions of $0 \leq t \leq 1$ are within 0.1 degree, the corresponding two curves are almost overlapped with each other. (b) Two types of tetrahedra showing the tilting angles Θ_1 and Θ_2. (c) An average of the two angles $(\Theta_1 + \Theta_2)/2$ with t. The tilting angles Θ_1 and Θ_2 in (a) are defined for two types of tetrahedra as illustrated in (b). As Θ_1 and Θ_2 are slightly different, an average of the two angles, $\Theta = (\Theta_1 + \Theta_2)/2$ in (c), is used as the tilting angle in discussion for simplicity. Phase parameter t is defined by $t = x_4 - \mathbf{q} \times \mathbf{r}$, where x_4 is the fractional coordinate of the 4th direction in (3 + 1)-dimensional superspace description, $\mathbf{q}$ is the modulation wavevector, and $\mathbf{r}$ is the positional vector. Figure S3: (a) Projection of a partial structure along the *a*-axis. (b) Enlargement of the structure, as indicated by an arrow in (a), showing the replacement of layer *S* with layer *S″*. (c) An example of the replacement of layer *T* with layer *T*.

Author Contributions: H.N. designed the experiments and wrote the paper; S.A. and K.K. performed the synthesis and PL experiments; Y.H., Y.M., N.H., and K.F. analyzed the XRD using the RIETAN-FP and JANA programs. All authors have read and agreed to the published version of the manuscript.

Funding: Part of this research was funded by NIMS Joint Research Hub Program FY2019.

Acknowledgments: We thank K. Kondo of the Nagoya Institute of Technology for his technical assistance in XRD.

Conflicts of Interest: The authors declare no conflict of interest.

Crystal Structure Data: We deposited the crystal structure data of the IC-phase at the Cambridge Crystallographic Data Centre, which were assigned the number CCDC 1961703.

References

1. Choi, S.-W.; Hong, S.-H. Characterization of Ca_2SiO_4: Eu^{2+} phosphor synthesized by polymeric precursor process. *J. Am. Ceram. Soc.* **2009**, *92*, 2025–2028. [CrossRef]
2. Luo, Y.Y.; Jo, D.S.; Senthil, K.; Tezuka, S.; Kakihana, M.; Toda, K.; Masaki, T.; Yoon, D.H. Synthesis of high efficient Ca_2SiO_4:Eu^{2+} green emitting phosphor by a liquid phase precursor method. *J. Solid State Chem.* **2012**, *189*, 68–74. [CrossRef]
3. Zhang, Y.; Chen, J.; Li, Y.; Seo, H.J. Monitoring of hydroxyapatite conversion by luminescence intensity of Eu^{3+} ions during mineralization of Eu^{3+}-doped β-Ca_2SiO_4. *Opt. Mater.* **2014**, *37*, 525–530. [CrossRef]
4. Wei, F.; Jia, Q. Massive production of A_2SiO_4:Eu^{3+} and A_2SiO_4: Eu^{2+} (A = Ca, Sr, Ba) microspheres and luminescent properties. *Superlattices Microstruct.* **2015**, *82*, 11–17. [CrossRef]
5. Sato, Y.; Kato, H.; Kobayashi, M.; Masaki, T.; Yoon, D.H.; Kakihana, M. Tailoring of deep-red luminescence in Ca_2SiO_4: Eu^{2+}. *Angew. Chem. Int. Ed.* **2014**, *53*, 7756–7759. [CrossRef] [PubMed]
6. Furuya, S.; Nakano, H.; Yokoyama, N.; Banno, H.; Fukuda, K. Enhancement of photoluminescence intensity and structural change by doping of P^{5+} ion for $Ca_{2-x/2}(Si_{1-x}P_x)O_4$: Eu^{2+} green phosphor. *J. Alloy. Compd.* **2016**, *658*, 147–151. [CrossRef]
7. Nakano, H.; Yokoyama, N.; Banno, H.; Fukuda, K. Enhancement of PL intensity and formation of core-shell structure in annealed $Ca_{2-x/2}(Si_{1-x}P_x)O_4$:$Eu^{2+}$ phosphor. *Mater. Res. Bull.* **2016**, *83*, 502–506. [CrossRef]
8. Nakano, H.; Kamimoto, K.; Yokoyama, N.; Fukuda, K. The effect of heat treatment on the emission color of P-doped Ca_2SiO_4 phosphor. *Materials* **2017**, *10*, 1000. [CrossRef]
9. Nakano, H.; Ozono, K.; Hayashi, H.; Fujihara, S. Synthesis and luminescent properties of a new Eu^{3+}-doped $Li_{1+x}(Ta_{1-z}Nb_z)_{1-x}Ti_xO_3$ Red phosphor. *J. Am. Ceram. Soc.* **2012**, *95*, 2795–2797. [CrossRef]
10. Ichioka, H.; Furuya, S.; Asaka, T.; Nakano, H.; Fukuda, K. Crystal structures and enhancement of photoluminescence intensities by effective doping for lithium tantalate phosphors. *Powder Diffr.* **2015**, *30*, 326–332. [CrossRef]
11. Taylor, H.F.W. *Cement Chemistry*, 2nd ed.; Thomas Telford: London, UK, 1997.

12. Fukuda, K.; Maki, I.; Ito, S. Thermoelastic behavior in Ca_2SiO_4 solid solutions. *J. Am. Ceram. Soc.* **1996**, *79*, 2925–2928. [CrossRef]
13. Fukuda, K.; Maki, I.; Ito, S. Thermal hysteresis for the $\alpha_L' \leftrightarrow \beta$ transformations in strontium oxide-doped dicalcium silicates. *J. Am. Ceram. Soc.* **1996**, *79*, 2969–2970. [CrossRef]
14. Fukuda, K.; Maki, I.; Ito, S.; Miyake, T. Structural change in phosphorus-bearing dicalcium silicates. *J. Ceram. Soc. Jpn.* **1997**, *105*, 117–121. [CrossRef]
15. Jost, K.H.; Ziemer, B.; Seydel, R. Redetermination of the structure of β-dicalcium silicate. *Acta Crystallogr.* **1977**, *33*, 1696–1700. [CrossRef]
16. Lu, X.; Wang, S.; Liu, S.; Du, P.; Ye, Z.; Geng, X.; Cheng, X. Phase identification of γ- and β-Ca_2SiO_4 via the rear-earth fluorescence probe. *J. Phys. Chem. C* **2019**, *123*, 13877–13884. [CrossRef]
17. Saalfeld, H.; Klaska, K.H. The crystal structure of 6 $Ca_2SiO_4 \cdot 1Ca_3(PO_4)_2$. *Z. Kristallogr.-Cryst. Mater.* **1981**, *155*, 65–73. [CrossRef]
18. Fukuda, K.; Maki, I. Transitional phase of Ca_2SiO_4 solid solution with incommensurate superstructure. *J. Am. Ceram. Soc.* **1989**, *72*, 2204–2207. [CrossRef]
19. Fukuda, K.; Maki, I.; Ito, S.; Yoshida, H.; Aoki, K. Structure and microtexture changes in phosphorous-bearing Ca_2SiO_4 solid solutions. *J. Am. Ceram. Soc.* **1994**, *77*, 2615–2619. [CrossRef]
20. Hiramatsu, Y.; Michiue, Y.; Funahashi, S.; Hirosaki, N.; Banno, H.; Urushihara, D.; Asaka, T.; Fukuda, K. Crystal structure and photoluminescence properties of an incommensurate phase in EuO- and P_2O_5-doped Ca_2SiO_4. *Inorg. Chem.* **2019**, *58*, 6155–6160. [CrossRef]
21. Smaalen, S.V. *Incommensurate Crystallography*; Oxford University Press: New York, NY, USA, 2007.
22. Janssen, T.; Chapuis, G.; de Boisseu, M. *Aperiodic Crystals*; Oxford University Press: New York, NY, USA, 2007.
23. Rietveld, H.M. Line profiles of neutron powder-diffraction peaks for structure refinement. *Acta Crystallogr.* **1967**, *22*, 151–152. [CrossRef]
24. Brindley, G.W. The effect of grain or particle size on X-ray reflections from mixed powders and alloys, considered in relation to the quantitative determination of crystalline substances by X-ray methods. *Philos. Mag.* **1945**, *36*, 347–369. [CrossRef]
25. Izumi, F.; Momma, K. Three-dimensional visualization in powder diffraction. *Solid State Phenom.* **2007**, *130*, 15–20. [CrossRef]
26. Udagawa, S.; Urabe, K.; Yano, T.; Takada, K.; Natsume, M. Studies on the Dusting of Ca_2SiO_4—The Crystal Structure of α'_L-Ca_2SiO_4. *Proc. Jpn. Cem. Eng. Assoc.* **1979**, *33*, 35–37.
27. Petricek, V.; Dusek, M.; Palatinus, L. Crystallographic computing system JANA 2006: General features. *Z. Kristallogr.-Cryst. Mater.* **2014**, *229*, 345–352. [CrossRef]
28. Momma, K.; Isumi, F. VESTA 3 for three-demensional visualization of crystal, Volumetric and morphology data. *J. Appl. Crystallogr.* **2011**, *44*, 1272–1276. [CrossRef]
29. Balic-Zunic, T.; Vickovic, I. IVTON—A program for the calculation of geometrical aspects of crystal structures and some crystal chemical applications. *J. Appl. Crystallogr.* **1996**, *29*, 305–306. [CrossRef]



© 2019 by the authors. Licensee MDPI, Basel, Switzerland. This article is an open access article distributed under the terms and conditions of the Creative Commons Attribution (CC BY) license (http://creativecommons.org/licenses/by/4.0/).